BioMedical Engineering OnLine

RESEARCH

Open Access

Evaluation of stiffness-matched, 3D-printed, NiTi mandibular graft fixation in an ovine model

Nada Raafat Khattab[1,2], Luis H. Olivas-Alanis[1,3], Agnieszka Chmielewska-Wysocka[4], Hany Emam[5], Ryan Brune[6], Ahmadreza Jahadakbar[7,8], Sahil Khambhampati[1], Joseph Lozier[9], Keyvan Safaei[7,10], Roman Skoracki[2], Mohammad Elahinia[7] and David Dean[1,2,11*]

*Correspondence:
David.Dean@osumc.edu

[11] Department of Materials Science and Engineering, Department of Plastic and Reconstructive Surgery, The Ohio State University, 460 West 12th Ave., Rm. 388, Columbus, OH 43210, USA
Full list of author information is available at the end of the article

Abstract

Background: Manually bent, standard-of-care, Ti–6Al–4V, mandibular graft fixation devices are associated with a significant post-operative failure rate. These failures require the patient to endure stressful and expensive re-operation. The approach recommended in this report demonstrates the optimization of graft fixation device mechanical properties via "stiffness-matching" by varying the fixation device's location, shape, and material composition through simulation of the device's post-operative performance. This provides information during pre-operative planning that may avoid future device failure. Optimized performance may combine translation of all loading into compression of the bone graft with the adjacent bone segments and elimination or minimization of post-healing interruption of normal stress–strain (loading) trajectories.

Results: This study reports a sheep mandibular graft model where four animals received virtually optimized, experimental nickel–titanium (NiTi) fixation plates fabricated using laser beam powder bed fusion (LPBF) additive manufacturing (AM). The last animal, our control, received a standard-of-care, manually bent, Ti–6Al–4V (aka Ti64) fixation plate. A 17.5-mm mandibular graft healed completely in all four animals receiving the experimental device. Experimental NiTi-implanted sheep experienced mandibular bone healing and restoration. The Ti64 plate, in the control animal, fractured and dislocated shortly after being implanted.

Conclusion: The use of stiffness-matched implants, by means of plate material (NiTi) and geometry (porosity) enhanced bone healing and promoted better load transfer to the healed bone when compared to the bulk Ti64 found in the fixation plate that the Control animal received. The design technique and screw orientation and depth planning improved throughout the study leading to more rapid healing. The large animal model reported here provides data useful for a follow-on clinical trial.

Highlights

- Novel stiffness-matching approach to skeletal fixation ensuring compression of bone fragments.
- Standard-of-Care Ti–6Al–4V device shown to fail quickly in this and another recent study.

- Less stiff NiTi material and designed porosity facilitate stiffness modulation.
- Stiffness-matched mandibular graft fixation hardware demonstrates full healing in this sheep model.
- Personalized fixation location, shape, and material show potential to improve patient outcomes.

Keywords: Additive manufacturing, Stress shielding/stress concentration, Nickel–titanium, Virtual surgical planning, Sheep model

Graphical Abstract

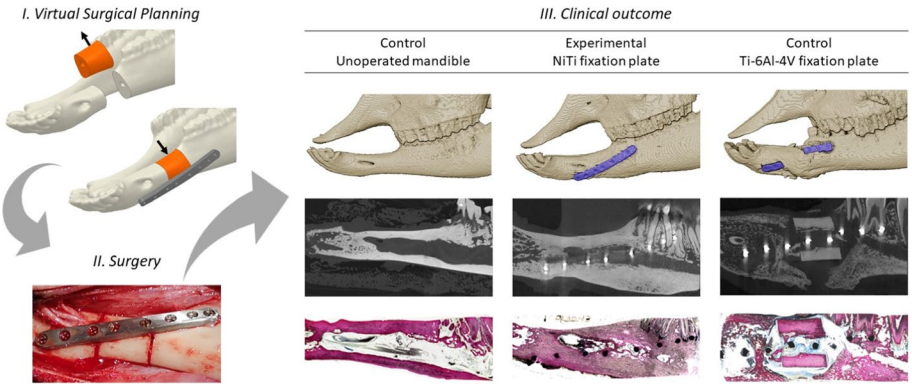

Background

When a bone fixation or replacement device failure occurs, it is often attributed to overly stiff materials that may have led to stress shielding-induced bone resorption (loss), implant loosening, and eventually device failure [1, 2]. The most commonly used fixation material is Surgical Grade 5 titanium alloy, Ti–6Al–4V (aka Ti64) [3]. This material has a much higher Young's modulus (i.e., an index of the material's stiffness) (112 GPa) than the surrounding mandibular cortical bone (10–31 GPa) [4, 5]. Furthermore, another possible cause of failure is stress concentration in the implant, especially in work-hardened "crimp" (i.e., thinned areas for manual bending) zones. Studies of CMF fixation have observed that 36–39% of large-mandibular graft fixation devices are observed to have post-surgery complications, including plate exposure, screw loosening, or plate fracture. In many cases, this requires revision surgery [1, 6–8]. Even though continuous research into, and development of, improvements in bone fixation devices have reduced this complication rate, the risk of fixation plate failure remains high for large CMF (craniomaxillofacial) grafts [9]. Across all skeletal fixation devices, 8–10% of all fixation plates are observed to break [10], loosen [11], or in other ways fail during normal activities (i.e., no trauma). In addition to the painful and stressful emergency caused by an unexpected failure of CMF fixation devices, typical re-operation costs average $50,000 [12]. The lack of biomechanical data makes it difficult for attending physicians to avoid stress shielding or to predict device performance.

Virtual surgical planning (VSP) is a common tool employed for reconstructive CMF surgery. This approach allows for detailed surgical planning, on computational

platforms, and provides valuable insight and preparation for actual surgical procedures. In most VSP environments one can obtain the target shape of a fracture or a segmental defect site to be reconstructed, as well as identify sites for fixation hardware placement. The size and shape of a bone graft or flap used to fill a segmental defect can also be visualized. Currently, it is common that a model of the virtually reconstructed bone is additively manufactured (also known as 3D printed), and fixation plates are manually bent to that model to provide an optimal fit. As an alternative to a manually bent fixation plate, it is now common to 3D print masticatory load-bearing, VSP-designed, CMF fixation plates. This level of personalization ensures that the plate will be uniformly flush to the bone, thereby increasing the overall reconstruction's stability [13, 14]. However, current VSP sessions rarely provide the surgeon with the fixation plate's anticipated post-operative mechanical performance [15]. Instead, surgeon decisions on fixation hardware geometry, material, or location are most commonly based on the surgeon's experience and medical judgment. Because there is virtually no biomechanical information available in current fixation design specifications provided to the physician, FDA clearance (e.g., testing conformance with standard-of-care device guidelines) relies on generic mechanical testing standards, e.g., ASTM F382-17, [16] as a basis to reduce the risk of fixation device mechanical failure. If biomechanical data were available during VSP, it could be used by the surgeon to choose the optimal fixation plate size, shape (i.e., external shape, internal porosity), location, and material, as well as screw location, type, and length.

Extending current VSP approaches to include information about implant geometry, location, and material, as well as screw location and length, one could then develop an optimal fabrication process for a personalized mandibular graft fixation plate. This is the workpath we took in the study reported here. Good fit and function of fixation hardware is expected to improve the sustainability and speed of healing, which may also be aided by the post-operative wound healing environment. That is because bone fractures, by virtue of hematoma formation from injured vessels, the early inflammatory response, and the cytokine cascade that follows the surgical "injury" (e.g., soft tissue incisions, osteotomies, etc.) start the healing process by creating an interplay between bone, endothelial, and inflammatory cells that ultimately can aid in bone regeneration and remodeling [17].

We hypothesize that informing surgeons' choices about a personalized fixation device's size, shape, material properties, and location is the best way to avoid both stress shielding-induced bone loss and stress concentration-induced fixation device failure [18]. This study involves the development of a mandibular fixation plate that is tailored to match the mechanical need for maintaining grafted bones in compression in response to all loads encountered during the healing period.

Furthermore, a superelastic nickel–titanium (NiTi) alloy was selected as the material for the studied fixation plates due to its low Young's modulus, between 28 and 70 GPa (austenite: 70 GPa; martensite: 28–40 GPa), which is significantly less stiff than the conventionally used Ti–6Al4V, and its unique property of superelasticity, with up to 8% of recoverable elongation without breaking [19]. Several works have reported the use of Ni-rich NiTi alloy for additively manufactured biomedical devices. The current application of this material in medical devices is only for small wire-like components, such as stents and wires [20]. Even though Ni ions are known to be cytotoxic, studies have shown that

the maximum Ni ion release rate of 3D-printed parts in physiological conditions is comparable to that observed in conventional NiTi devices [21]. Furthermore, it was proven that the leached Ni in solid and porous 3D-printed NiTi is too low to promote cytotoxicity [5, 22]. For example, good biocompatibility and inert activity of 3D-printed NiTi samples implanted in the frontonasal bone was recently demonstrated in a porcine model [23].

To evaluate the benefit of our VSP-engineered mandibular graft fixation plates, bone healing was compared to the gold standard, a hand-bent Ti64 fixation plate. Mandibular fixation plates were implanted in five sheep which underwent mandibular osteotomy to create a bone defect. Four were fitted with NiTi fixation plates and one serving as a control was fitted with a manually bent, conventional Surgical Grade 5 titanium alloy mandibular graft fixation plate.

Results

Clinical outcomes

All four animals that received experimental NiTi fixation plates made a successful recovery following their surgical procedures and displayed indications of good overall well-being during their post-operative healing period. Interestingly, the experimental sheep #2 plate eventually failed (broke) at the sixth screw (posterior to anterior) position. Nevertheless, the animal experienced full bone healing and restoration. There was a gradual improvement in the healing seen in each experimental animal's osteotomy bone graft and in any surrounding callus that developed. There was no evident pain, and sheep weight fluctuation was not out of the expected range, according to the attending veterinarians. Neither the control, nor the experimental, sheep had significant clinical observations during the study period. Complications in the form of infection, inflammation, or dehiscence were not observed. The adversities sheep encountered were negligible, which included difficulty adjusting to the weather as their fur grew after each shear and some skin abscesses that healed rapidly. There were no notable changes in behavior, physical symptoms, or any signs of illness or distress observed in the sheep. 3D CT reconstruction images revealed that all four experimental sheep showed successful bone graft healing with modest callus formation (Fig. 1). All of the callus formation was fully resolved through bone remodeling. The osteotomy site in the experimental animals showed rapid bridging followed by full restoration of original bone anatomy, as shown on clinical 3D

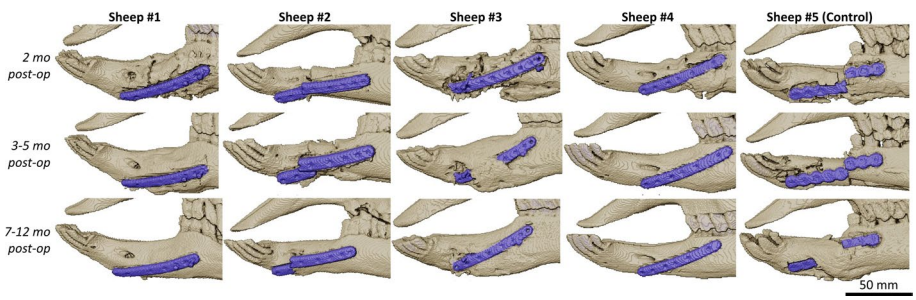

Fig. 1 3D CT reconstructions of the healing process of experimental animals 1–5 at three different time points across the study: top row—within 2 months after surgery; middle row—3–5 months after surgery healing time; bottom row—final image before sacrifice

CT. As mentioned, experimental sheep #2 exhibited late (post-healing) plate breakage which appeared to not affect the animal. Even though careful VSP was undertaken, Animals #1 and #3 showed screw loosening, which was suspected to be due to those screws not being bicortical. Rapid and uneventful healing was observed in sheep #4, as the VSP process and learning curve appear to have enhanced our results as the study proceeded.

On the other hand, the control animal, sheep #5, while not judged to be in distress after its plate broke, did at times show withdrawn behavior, and jaw clicking while chewing/ruminating. This was due to a broken fixation plate, unresolved callus, and dislocated bone (Fig. 1). Indeed, the Ti–6Al–4V fixation plate received by the control animal fractured within a month of surgery, resulting in a significant jaw dislocation. That animal developed a large callus that did not resolve.

Micro-CT and histology

Representative images from micro-CT and histology for all studied animals are shown in Fig. 2. Both methods depict bone growth and integration at the sites of screws in sheep #1–4, and a lack of healing in sheep #5. The histology shows that all of the experimental animals display a consistent and uniform, well-healed host–graft bone interface, characterized by abundant pink coloration due to Sanderson's Rapid Bone Stain which has been counterstained with Van Gieson stain. The histology for the control animal, sheep #5, exhibited morphology consistent with the presence of fibrous tissue (i.e., blue stain in unhealed callus region seen in Fig. 2). The absence of a consistent and orderly arrangement of bone tissue implies a lack of successful progress in achieving normal healing in the control animal.

Discussion

Restoring the mandible's shape and functionality after bone resection due to trauma or cancer is the main objective of reconstructive surgery. Even though the use of titanium plates is the gold standard for bone graft fixation, clinical outcome reports show a high rate of device failure, mainly due to a stress shielding effect (i.e., bone loss) [24]. The clinical significance of stress shielding varies with the shape, material, and location of fracture fixation hardware. Specifically, areas bearing high loads, such as the mandible, lower spine, or the femur, are more prone to experience unbalanced stress following the addition of localized, very stiff fixation hardware. We have recently noted [25] that a stiffness-matching approach might be able to restore a bone's normal function during healing through treating the whole functional unit while simultaneously reducing osteotomy site motion. With the addition of biomechanical information, one can simulate loading both during and after healing. That simulation can help the surgeon attempt to avoid interrupting normal post-healing loading, a potential cause of stress shielding, as much as possible. This study focused on optimizing implant (i.e., plate and screws) material, geometry, and location to address these concerns by enhancing bone healing and by tailoring the fixation strategy to the specific demands of the implant site and the functional unit during and after healing.

The results presented in this report expose secondary problems currently seen in patients when using off-the-shelf, standard-of-care mandibular graft fixation plates [26]. Sheep #5 (control), which received a Ti64 hand-bend plate, demonstrated subpar

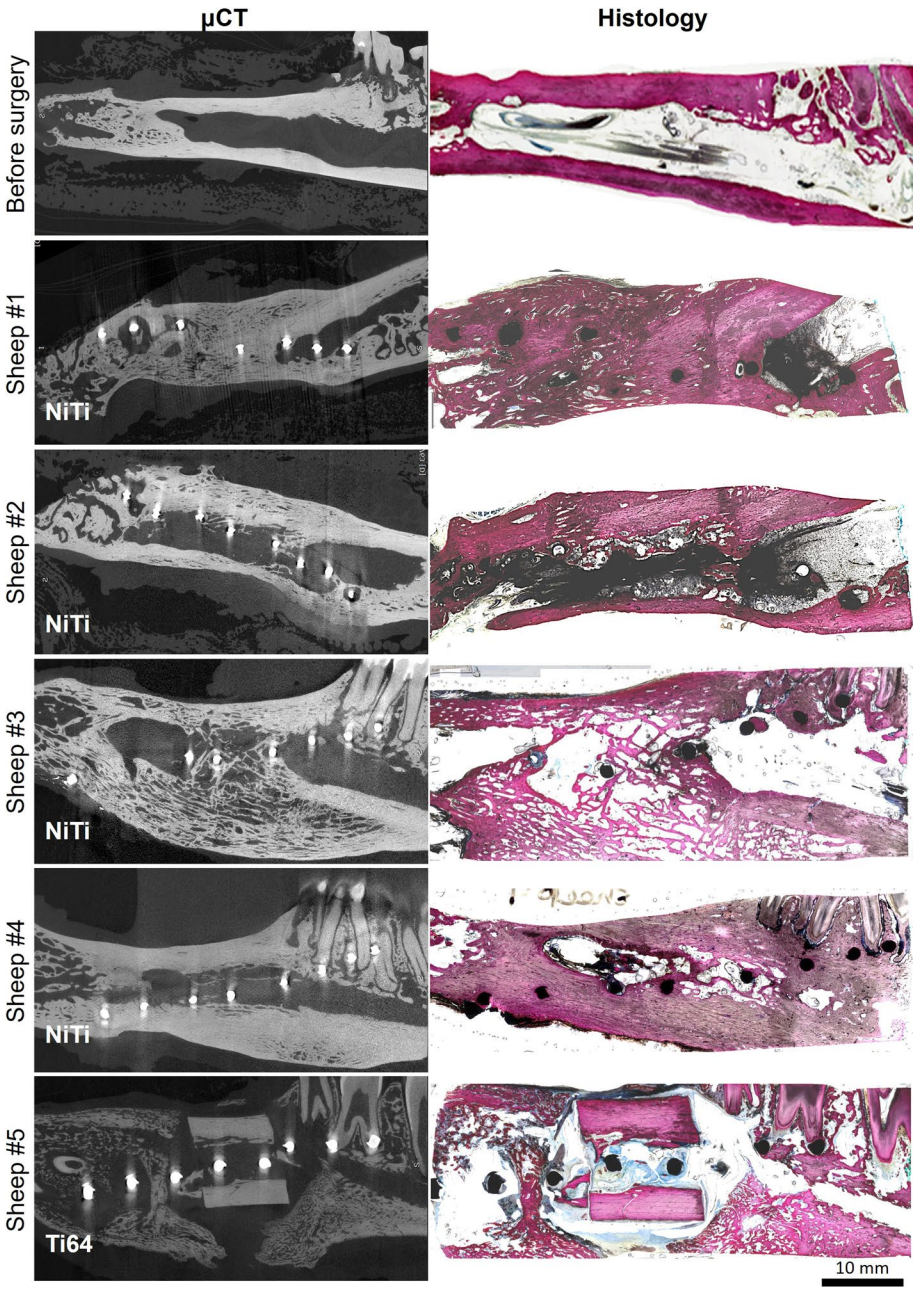

Fig. 2 Matching sagittal micro-CT and histology images of explants taken from all animals at the end of the study. The histology was prepared using hard plastic embedding which was then stained with Sanderson's Rapid Bone Stain and counterstained with Van Gieson stain. Sheep #1–4 display fully healed mandible bone grafts whereas the control animal (#5) shows non-union and a lack of pink/red stain seen in areas of undisturbed and fully healed bone. Instead, one sees blue-stained regions which indicate soft fibrous, cartilage tissues

performance and encountered difficulties in achieving standard healing and regular chewing, marked by clicking noises and irregular chewing motions. Similar results were observed by Pérez-Basterrechea et al. when implanting a serum-based scaffold loaded with bone marrow-mesenchymal stem cells (BM-MSCs) in a sheep model [26].

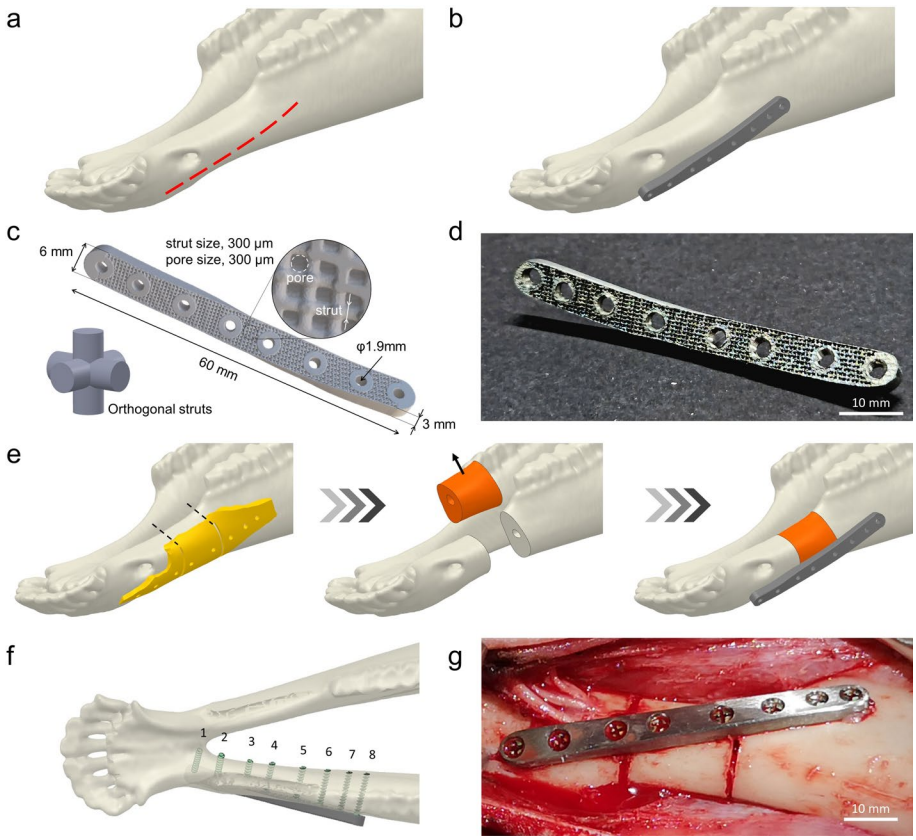

Fig. 3 **a** Surface detection for an osteotomy in a diastema region. **b** Design of NiTi stiffness-matched mandibular graft fixation plate. **c** Mandibular plate geometry and orthogonal strut porous infill showing unit cell architecture. **d** Image featuring LPBF additively manufactured stiffness-matched NiTi fixation plate for engrafted mandible. **e** Osteotomy VSP: from the left-cutting guide (dashed lines demonstrate osteotomy planes), osteotomy of diastema region, engrafted sheep mandible. **f** VSP of screw location and length; screws 1–3 are located in anterior bone; screws 4 and 5 are located in bone graft; screws 6–8 are located in posterior bone. **g** Intraoperative image featuring a NiTi fixation plate that has been successfully attached to the sheep's mandible

They found that, even though some level of mandibular bone formation was achieved, there was observed callus and fibrous tissue formation, incomplete bone consolidation, and unsuccessful restoration of the mandibular contour. At the time of euthanasia, the plate was found fractured along with loose screws. This was attributed to the high stiffness of the implanted Ti–6Al–4V plate (2.6 mm thick), which acted as a load bypass and experienced high-stress concentration. Furthermore, it provoked suboptimal mechanical stimulation and hindered bone remodeling. Another recent study attempted to use standard-of-care Ti–6Al–4V fixation plates in a sheep mandibular segmental defect model. As with the control animal in our study, plate fracture was rapid (within 4 weeks). That study corrected the problem of plate fracture with the addition of a second, larger, plate [27].

Manually bent, off-the-shelf fixation plates often have crimping areas that are located between all the screw-eyes. This compromises the elasticity of the plate in these areas, especially if there is repeated bending to reach the required form-fitting shape. Repeated

bending may cause work hardening at the repeatedly-bent crimp sites. Work-hardened sites may be prone to fatigue (i.e., cyclic loading) failure [15]. Previous work has shown, with statistical significance, differences in hardness between manually bent and pre-bent plates, bent optimally to fit a surgical planning model. The former has lower hardness as it experiences excessive bending and twisting deformation [28]. Additionally, computational models that minimize pre-bending stress and screw tightening may reduce susceptibility to plate fracture [29].

In contrast, all of the experimental sheep, which received an engineered personalized 3D-printed NiTi fixation plate, showed satisfactory recovery. The clinical 3D CT, micro-CT, and histology findings suggest that bone healing progressed similarly and normally for all experimental animals throughout the study. Therefore, the optimization of mechanical properties and geometry, coupled with precise location planning of the NiTi bone fixation plate and screws, has likely reduced, if not eliminated, the negative outcomes associated with bone stress shielding and device stress concentration. Towards counterattacking the stress shielding effect, previous works have reported the use of novel materials for custom made mandibular plates [30]. A common example is polyetheretherketone (PEEK) since the material shows biocompatibility and increased elasticity. As with NiTi, PEEK implants can be additively manufactured, making it possible to produce complex and personalized shapes. However, it is known that PEEK is bioinert and may not provide optimal osseointegration. Furthermore, it has not been fully reported as to whether the PEEK fixation plates studied can withstand chewing forces [30, 31]. We expect that our approach of using a single plate of similar size to, but much less stiff than the standard-of-care, was successful because, as noted in the "Micro-CT and histology" section (above), we model the effect of maximum chewing load on the osteotomy site based on the fixation plate's location, geometry, and material [32, 33]. Our mechanical model shows that a less stiff implant is less likely to concentrate stress at a highly localized area of the fixation plate or on a particular screw. We hypothesize that this is because the less stiff plate can engage all of the screws, the remainder of the plate, and the adjacent bone segments (i.e., the healing bone functions more like the normal bone). Additionally, careful choice of the location of a fixation plate can better ensure that the load results primarily in compression at the osteotomy sites and that micromotion at those sites is kept below 300–400 μm [34]. Finally, we anticipate that our VSP approach is capable of minimizing the time of callus formation and resolution, as well as the time of bone healing through improved device placement and locking, bicortical screw planning, all of which resulted in contour restoration.

Despite the improved healing seen in the experimental sheep, one out of these four sheep (animal #2) exhibited late (post-healing) plate breakage. This complication was not deemed a failure, as the bone healed normally. We attribute this to the difference in size of that animal compared to the other ones. Although it was chosen from the same herd, it was significantly smaller than the other four animals, but similar in its craniofacial morphology. Furthermore, the same contoured 3D-printed plate was used for all four experimental sheep, assuming that the strain would present similarly given constant craniofacial morphology. While the graft fixation plate fit Sheep #2 well at surgery, some minor adjustment was required to situate the fixation plate. Sheep #2 was healing in the expected manner until it was observed via 3D CT that the fixation plate had

broken into two pieces. Subsequently, these two pieces moved further away from each other. We hypothesize that as the healthy loading of the mandible was progressively restored, and the NiTi plate already completed its work, the remodeling of bone and increased chewing strength broke the flexible NiTi fixation plate. This behavior has been explored in recent in silico studies. Wan *et al*., showed that the increasing occlusal load, due to progressive bone healing and remodeling, could promote the fracture of a fixation plate due to fatigue failure [35].

While the results are promising, this study has a few limitations. Animal experiments involve uncontrollable variables, such as differences in healing rates due to genetics and age. We minimized this by selecting sheep of the same strain with similar characteristics. Sheep's social nature can impact recovery. Therefore, we adhered to standard sheep protocols to reduce stress and provide enrichment. Furthermore, even though the selection of a very small sample size for the control group could jeopardize the analysis, the study was planned based on the reported literature and adhering to the 3R ethical considerations: Replacement, Reduction, and Refinement [36]. Thus, once it was confirmed that an optimal plan with a standard-of-care fixation plate would not work, it was not appropriate to make another animal undergo a broken fixation plate.

Finally, it may be useful to consider the corrosive potential of using NiTi (fixation plate) and Ti64 (screws) components in a single fixation device. The employment of different metals could lead to metal degradation due to galvanic corrosion. In this study, we did not observe corrosion on the explanted components. We hypothesize that little to no corrosion occurred due to the minute difference in electrical potential between NiTi and Ti64 (0.2 V) [37, 38] and the fact that both materials tend to form a passive, protective TiO_2 layer which could reduce or even negate the possibility of galvanic corrosion [39, 40]. However, to our knowledge, the galvanic interaction of these two metals has not been previously reported and should be evaluated.

Conclusions

This study presents a novel stiffness-matching approach for bone fixation plates. Stiffness is not only reduced by choosing NiTi over Ti–6Al–4V or by matching stiffness to the adjacent bone. Rather, the stiffness of the overall construct (i.e., adjacent host bone, grafted bone, screws, and fixation plate) is designed to accomplish the work of maintaining compression between adjacent healing bone segments under all loads during bone healing. That work is facilitated by planned (i.e., biomechanically modeled and optimized) engagement of the full mechanical segment composed of the fixation plate, screw, and bone fragment in order to reduce osteotomy site micromotion and speed bone healing. Given that this strategy has now proven successful in a large animal mandibular graft model, it indicates that the approach shows promise for clinical mandibular graft and skeletal reconstruction applications.

The overall observation is that a well-placed, stiffness-matched, fixation plate brings the following benefits:

(1) Reduced stiffness allows better engagement of the whole fixation plate and all of the screws, thereby avoiding stress concentrations.

(2) Better engagement of the whole fixation plate and accurate screw planning reduces screw loosening. Better screw planning ensures that screws adjacent to a heavily loaded screw are not loosened. Instead, they are tightened.
(3) Screw stability is enhanced through accurate bicortical screw placement and modulating screw orientation (i.e., not all in the same plane). Screw orientation is further enhanced when the fixation plate is designed, if possible, to wrap around the bone.
(4) Designing the fixation plate to wrap around the bone helps keep the host and graft bone fragments in compression during loading, which is likely to speed the healing process.

We anticipate that a biomechanically informed VSP session that simulates post-operative performance can optimize screw planning as well as the surgeon's choices of fixation plate location, size, shape (i.e., internal pore geometry and external surface shape), and material. In addition to providing cutting guides or intra-operative guidance to deploy personalized fixation, VSP that includes biomechanical modeling can help minimize fixation hardware interruption of normal stress–strain trajectories once the grafted bone has fully healed in place. Allowing restoration of normal loading should avoid future stress shielding-induced bone loss or stress-concentration-induced device failure, especially cyclic loading-induced failure.

Materials and methods

Virtual surgical planning (VSP): skeletal geometry and biomechanical input into fixation shape and location decisions

A useful biomechanical model for VSP should consider all of the components involved, such as host bone, bone graft or grafts that fill(s) a defect, and the graft fixation device. Additionally, the structural performance of the assembly should then be evaluated under the anticipated chewing forces. This comprehensive analysis assists in the selection of suitable hardware shape, location, and material properties, thereby preventing harmful stress shielding of the adjacent bone and stress concentrations within the device. To create this model, an outer surface image of the skull and mandible, derived from a 3D computed tomography (CT) image, was converted to a solid object composed of a tetrahedral mesh with assigned mechanical properties (i.e., a finite element model or FEM). The geometry and mechanical properties of the masticatory anatomy that is to be surgically reconstructed can be directly derived from 3D CT data [41]. This approach aims to design a personalized fixation device that facilitates bone graft and adjacent host bone healing, while not interrupting, or minimally interrupting, the normal masticatory stress–strain trajectories of the bone once it has healed.

VSP: biomechanical input into material choice and shape modulation

The initial step in the modeling process entails detecting the surface where the fixation plate will be positioned (Fig. 3a), followed by the precise modeling of the fixation plate to ensure that it sits flush with the bone surface (Fig. 3b).

The methods for the creation of a personalized model of mastication based on a 3D CT image have been presented in our previous work [32]. The model simulates the

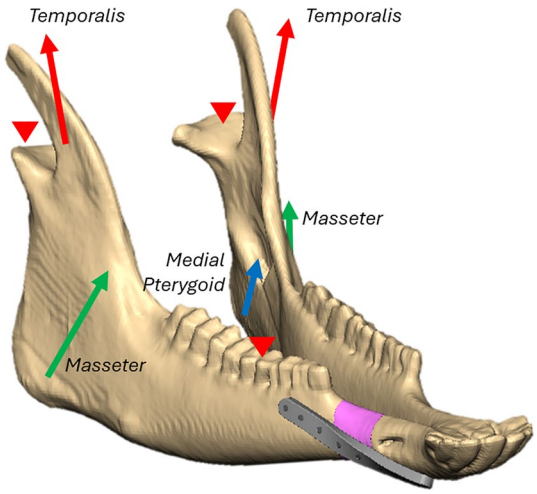

Fig. 4 Finite element model representing the direction of the three main masticatory muscles (masseter, medial pterygoid and temporalis), and the motion restraint points (condyles and first molar)

maximum chewing force at the M1 on the treated side, as seen in Fig. 4. This task begins with obtaining masticatory muscle vectors (i.e., the direction of pull) and force magnitude (i.e., chewing strength). The muscles considered for the model are masseter, medial pterygoid and temporalis (Fig. 4). Muscle force magnitude is directly inferred from the maximum cross-sectional area of each muscle [42]. Furthermore, the effect of the condylar process is simulated by restraining the motion at the mandibular condyles. Next, a model for maximum occlusal force is simulated based on biomechanical data [43–45]. Then, the design of a personalized fixation plate is evaluated in this biomechanical model to simulate the surgical outcome and make the best selection. Stress concentrations occurring in thin areas of a fixation device or a gap between the plate and the bone surface are to be avoided.

The objective of this study was to restore the normal loading patterns, once the bone has healed, despite the presence of CMF fixation, which is solely intended to secure the bone graft during the healing process with the host bone. The fixation must be stronger than the surrounding bone, to hold it in place while healing. Nevertheless, it must also possess enough flexibility to fully engage the entire plate and all of the screws needed to maintain compression between the graft and adjacent bone, with minimal micromotion at the osteotomy sites, under all loads. It has been reported that micromotion at the osteotomy (healing) sites must be kept under 300–400 μm [34].

Sheep model: polled Dorset sheep

In this study, our human simulation of mastication was translated to a sheep model for mandibular graft fixation [46]. This animal model takes advantage of the fact that the diastema region of the sheep mandible can be removed and immediately placed back without removing teeth (Fig. 3), as would be required with most other relevant large mammal models. In addition, it allows the dimensions of the fixation hardware to be similar to that used in humans. While the ossification centers of the sheep mandible are closed before birth [46], growth continues through the period when dental maturity is

obtained. The bone mineral composition of the sheep mandible and its rate of bone healing do not differ significantly from humans [47, 48]. Other researchers have used a sheep mandibular graft model to study the regeneration of load-bearing, skeletal, segmental defects (i.e., the osteotomized bone is replaced with a tissue-engineered artificial graft) [49–51].

This study involved the use of five polled Dorset sheep, with four animals serving as experimental subjects and one serving as a control. The polled Dorset strain of sheep used in this study was developed at North Carolina State University, while the sheep themselves were sourced from The Ohio State University (OSU) herd located in Wooster, OH, USA. Due to the notable variation observed between ewes and wethers compared to other strains, females were exclusively utilized for the study [37].

Sheep model: design and fabrication of personalized (shape, location, material properties), additively manufactured NiTi mandibular graft fixation plate performance

The personalized mandibular plate was designed in a VSP environment employing Materialise Mimics software (Leuven, Belgium). Sheep 3D CT scans were used to segment the mandibular bone and create a surface mesh. For the plate design, first, a 17.5-mm-long osteotomy was digitally performed on the left diastema of the mandible. That resected bone was then replaced in its original location, mimicking a bone graft. The location of the form-fitted plate was designed so that three screw holes were located on the host bone, anterior and posterior to the graft, and the two central screw holes were located at the bone graft. Hence, the plate began posterosuperiorly to the graft, immediately anterior to the first premolar roots, then curved down to the inferior border of the mandible immediately anterior to the graft. This "wrap-around" geometry of the plate helps ensure that loading will bring about compression, rather than tension or spreading, at the osteotomy sites. The design of the fixation plate involved virtual screw planning to ensure maximum capture of the mandibular cortices (i.e., bicortical) proximal and distal to all screw heads (Fig. 3f). The designed plate is 3 mm thick, which is near the maximum thickness for current Ti–6Al–4V plates used in CMF reconstruction procedures, and 60 mm long.

In order to optimize the stiffness of the plate, our basic design for these fixation plates considers two components: (a) an outer solid "shell" with threaded, countersunk, solid screw-eyes for Ti–6Al–4V locking screws (provided by KLS Martin, Tuttlingen, Germany) and (b) an internal porous "core", where the pore geometry is used to modulate stiffness (Fig. 3c). The level of porosity was determined by using the previously described biomechanical model of chewing [32], with maximum occlusion at the first molar of the engrafted sheep mandible, provoked by the three muscles responsible for mandible clenching: masseter, pterygoid, and temporalis. The FEM was built and solved in ABAQUS software (Dassault Systèmes, Waltham, MA). The mechanical properties (e.g., elastic modulus) of the plate were varied to obtain an optimal micromotion for bone healing. According to the literature, a maximum micromotion or 150 μm should be allowed for primary bone healing, either in the anterior or posterior osteotomy site (superiorly or inferiorly) [42]. However, this work aimed for a third of the micromotion threshold (50 μm) to neglect any effect due to model uncertainties. Ti64 and NiTi were modeled as linear and superelastic materials (user-defined material subroutine)

Table 1 Mechanical properties assigned to a hypothetical solid plate and the resulting micromotion seen at the osteotomy site

Plate	Bottom area micromotion, μm	Top area micromotion, μm
Bulk Ti64, 120 GPa	14	2.3
Bulk NiTi, 62.5 GPa	27	33
Bulk, 30 GPa	18	15.9
Bulk, 10 GPa	23.5	32.5
Bulk, 5 GPa	38	45
Porous plate (38%) Ti64, 120 GPa	32	37
Porous plate (38%) NiTi, 62.5 GPa	36	44

[52], respectively. Furthermore, theoretic materials with elastic modulus of 30, 10 and 5 GPa were evaluated. Once the micromotion goal is obtained, the pore and strut size of orthogonally oriented strut infill is selected and computationally assessed to meet the desired stiffness. The elastic modulus and preliminary FEM results are shown in Table 1. A hypothetical plate with a 5 GPa Young's modulus maintained a maximum interfragmentary motion of 45 μm. Based on previous work, an orthogonal structure, with struts of 300 μm diameter interspersed by 300 μm pores, shows a stiffness close to 5 GPa [52]. When the porous plate is evaluated, the interfragmentary motion results in 44 μm.

Sixteen of the same fixation plates were additively manufactured in a Phenix Systems PXM (3D Systems, Rock Hill, SC) laser beam powder bed fusion (LPBF) 3D printer. The NiTi powder used was Ni50.1-Ti Eckart TLS GmbH (Bitterfeld-Wolfen, Germany). The powder was sieved before printing to ensure a particle size range between 20 and 75 μm. The LPBF process was carried out under a laser power of 250 W and a layer thickness of 30 μm. After the AM process, the fabricated parts were post-processed via chemical polishing to enhance the accuracy of the porous infill (Fig. 3d) using the method shown in previous work [53]. Thread milling was done on a 5-axis CNC at Vertex Manufacturing (Cincinnati, OH, USA).

Following the fixation plate design and location, a personalized osteotomy cutting guide (Fig. 3e) for the 17.5-mm osteotomized bone flap was designed for the NiTi plates using computer-simulated osteotomy and screw hole sites. The osteotomy cutting guide was fabricated via Stereolithography (SLA) AM with sterilizable Formlabs BioMed Amber resin on a Formlabs SLA 3D printer (Formlabs, Somerville, MA, USA). The goal of the cutting guide is to aid the physician during the surgical procedure with bone cutting and locating screw sites so that the fixation plate will behave as simulated via FEA.

Surgical protocol

The mandibular graft fixation implantation surgeries of the five sheep specimens were performed by the same surgeon (HE). The surgical procedure involves cutting the bone while the screws and plate remain in position, thereby achieving a planned gap. The surgical procedure incorporated the use of four 3D-printed NiTi fixation plates and one standard-of-care, manually bent, Ti–6Al–4V fixation plate. These surgeries followed

Ohio State University IACUC-approved protocol #2019A00000143, "Additive Manufacture of Stiffness-Matched Mandibular Graft Fixation Hardware".

The procedure began after the sheep was anesthetized and intubated. Next, an orogastric tube was placed as a vent to control eructation. Sterile technique was followed beginning with the skin and fascia being incised to access the diastema region of the mandible. Using the aforementioned, personalized cutting guide, two lines orthogonal to the diastema were marked on the bone to guide the positions of the fixation screw holes, bone-cutting locations, and screws were marked and then the screw holes were tapped. Next, the fixation plate was screwed in place. This was followed by the use of an oscillating saw to perform the two osteotomies previously marked 17.5 mm apart in the diastema region of the left mandible. These two osteotomies completely freed the previously marked bone, which was used as the bone graft for later healing. The osteotomies were performed with careful attention to the inferior alveolar neurovascular bundle and tooth roots. After ensuring that there were no blood vessels injured; the periosteum, fascia, and skin were then sutured and closed in layers. The oral cavity was inspected for any unintended puncture wounds to the oral mucosa. The procedure was successfully executed in under four hours for all the five cases.

After surgery, each animal was given a clean and quiet space to rest and recuperate, promoting a conducive environment for healing. Post-operative care included regular check-ups, wound care, and pain management. The sheep were assessed regularly, three times per day for 2 days; two to three times on the third day; and at least once daily thereafter. The animals were carefully observed for any signs of complications or discomfort and wound and bone healing. Accordingly, adjustments were made to their treatment plan. Along with post-operative care and monitoring, the oral cavity was flushed daily with an antiseptic solution for at least 2 days. Animals were weighed monthly and then sedated for imaging. Given that many large-mandibular fixation plates fail from 1 to 3 years after implantation, the decision was made to allow specimens 3 and 4 to survive until 1 year [6].

Tracking post-operative bone healing

Graft healing was tracked using histological and 3D CT imaging. Post-operative 3D CT scans were taken within 3 months following surgery and periodically thereafter, as often as every 2 weeks, until complete healing was achieved. Fixation plate integrity, callus formation and retreat, and osteotomy bridging were carefully tracked via 3D CT.

Sacrifice and histology

Immediately following euthanasia, the engrafted mandible was dissected and preserved in formalin. Before shipping to the Orthopaedic Research Bioengineering Laboratory at Colorado State University (Ft. Collins, CO), for histological analysis, each mandible was cut in half in the sagittal plane. One control, an unoperated hemi-mandible, was processed, along with four experimental and one control hemi-mandible with a standard-of-care Ti–6Al–4V mandibular graft fixation plate and screws. Before histological processing, all hemi-mandibles were micro-CT-scanned at a resolution of 38 μm (Scanco vivaCT 80, Scanco USA Inc., Wayne, PA). Hard plastic embedding was performed.

Matching sagittal micro-CT views, and sections stained with Sanderson's Rapid Bone Stain and counterstained with Van Gieson stain, were prepared.

Non-decalcified histological sections were taken in the sagittal plane of all specimens. At least two sections were cut through each specimen with a band saw (Exakt 310, Exakt Technologies, Oklahoma City, OK, SN: 081). Initial sections were taken using a diamond blade bone saw (Exakt Technologies) at a thickness of approximately 300 μm. All sections were ground using microgrinders (Exakt Technologies, SNs: 0206 and 0274) to 60–70 μm thickness. Slides were stained with Sanderson's Rapid Bone stain which provides differentiation of cells within the section and allows detection of cartilage within the tissue, then counterstained using Van Gieson's stain that allows differentiation of collagen and detection of bone (immature woven bone and mature lamellar bone) within the section.

Abbreviations

3D CT	Three-dimensional computed tomography (X-ray) scan
AM	Additive manufacturing
CMF	Craniomaxillofacial
CNC	Computer numerical control
FDA	United States Food and Drug Administration
FEM	Finite element model
IACUC	Institutional Animal Care and Use Committee
ISO	International Standards Organization
LPBF	Laser powder bed fusion (i.e., metal powder-based 3D printing)
NiTi	Nickel titanium (aka nitinol)
STL	Standard tessellation language (aka standard triangle language)
Ti–6Al–4V	Surgical Grade 5 titanium alloy
VSP	Virtual surgical planning

Supplementary Information

The online version contains supplementary material available at https://doi.org/10.1186/s12938-024-01289-x.

Supplementary Material 1

Acknowledgements

The authors thank Saylor Priest and Jonathan Chestang for their help with sheep monitoring and non-sterile assistance with planning and executing sheep surgeries associated with this project. The authors also thank Kenzington Kottenbrock, Timothy Huang, Nafees Sathik, Anjali Senthilkumar, and Ethan Shin for their involvement in those same activities as well as image acquisition and analysis. The authors also thank Steven Rengers and Tim Warden of Vertex Manufacturing (Cincinnati, OH) for threading the 3D-printed NiTi fixation plates used in this study. Most micro-CT images and all histology were prepared by Dr. Ben Gadomski and Dr. Kirk McGilvray at Colorado State University. The authors are grateful to KLS Martin (Jacksonville, FL), and especially our KLS Martin on-site contact, Mr. Corey Redmond, for providing locking screws and control, Ti–6Al–4V fixation plates, for our study.

Author contributions

NRK: project administration, data curation, formal analysis, methodology, research, writing—original draft, review and editing, visualization, animal selection, husbandry, euthanasia, necropsy, explant harvesting, supervised 3D CT imaging sessions. LHOA: research, computational model analysis, writing—original draft, review and editing. AC: project administration, data curation, research, visualization, writing—original draft, review and editing. HE: supervision, research, methodology. RB: project administration, research, data curation, visualization. AJ: research, computational model analysis. SK: research, formal analysis, methodology, visualization. JL: research, methodology, visualization, animal selection, husbandry, euthanasia, necropsy, explant harvesting, supervised 3D CT imaging sessions. KS: research. RS: supervision, research, methodology. ME: conceptualization, supervision. DD: conceptualization, data curation, formal analysis, research, funding acquisition, methodology, project administration, resources, supervision, validation, visualization, writing—original draft, review and editing.

Funding

Partial support for this project was provided by a Technology Validation Startup Fund (TVSF) Phase II grant, #TECG20170372, from the Third Frontier (Development Office), State of Ohio. Partial support for this project was provided by a grant from RegenFix, LLC (Toledo, OH). Partial support was provided by the Departments of Materials Science and Engineering and Plastic and Reconstructive Surgery, The Ohio State University. The authors wish to acknowledge a President's Research Excellence (PRE) Catalyst grant "Hybrid Autonomous Point-of-Care Manufacturing" from The Ohio State University, an Ohio State University James Comprehensive Cancer Center (CCC) grant from the Biomedical Device

Initiative, an Ohio State University Cancer Engineering Center (Ohio State University James CCC and College of Engineering) Postdoctoral Fellowship, and a National Science Foundation Engineering Research Center grant (2133630) "Hybrid Autonomous Manufacturing Moving from Evolution to Revolution" (HAMMER).

Data availability
Data are provided within the manuscript or supplementary information files.

Declarations

Ethics approval and consent to participate
All animal experiments and tests were guided and approved by IACUC-approved protocol #2019A00000143.

Competing interests
LO, AC, RS, ME, and DD are inventors on pending and/or issued patents that underlie the work reported here and that are licensed by RegenFix, LLC. DD and ME own founders equity in RegenFix, LLC (Toledo, OH).

Author details
[1]Department of Materials Science and Engineering, The Ohio State University, 140 W 19th Ave., Columbus, OH 43210, USA. [2]Department of Plastic and Reconstructive Surgery, Ohio State Plastic Surgery, 915 Olentangy River Road, Columbus, OH 43212, USA. [3]School of Engineering and Science, Tecnologico de Monterrey, Av Eugenio Garza Sada 2501 Sur, Monterrey, NL 64849, Mexico. [4]Cardinal Stefan Wyszynski University in Warsaw, Multidisciplinary Research Center, Dziekanow Lesny, Poland. [5]Oral and Maxillofacial Surgery, The Ohio State University, 305 W. 12th Ave., Columbus, OH 43210, USA. [6]Center for Design and Manufacturing Excellence, The Ohio State University, Bevis Hall, 1080 Carmack Rd, Columbus, OH 43210, USA. [7]Department of Mechanical, Industrial and Manufacturing Engineering, University of Toledo, 2801 Bancroft St., Toledo, OH 43606, USA. [8]Confluent Medical Technologies, Fremont, CA, USA. [9]Department of Veterinary Clinical Sciences, The Ohio State University, 1900 Coffey Rd., Columbus, OH 43210, USA. [10]TA Instrument, New Castle, DE, USA. [11]Department of Materials Science and Engineering, Department of Plastic and Reconstructive Surgery, The Ohio State University, 460 West 12th Ave., Rm. 388, Columbus, OH 43210, USA.

Received: 10 June 2024 Accepted: 3 September 2024
Published online: 26 October 2024

References

1. Zhang M, Gregory T, Hansen U, Cheng C. Effect of stress-shielding-induced bone resorption on glenoid loosening in reverse total shoulder arthroplasty. J Orthop Res. 2020;38(7):1566–74.
2. Eidel B, Gote A, Fritzen CP, Ohrndorf A, Christ HJ. Tibial implant fixation in TKA worth a revision?—how to avoid stress-shielding even for stiff metallic implants. Comput Methods Biomech Biomed Eng. 2021;24(3):320–32.
3. Spencer KR, Sizeland A, Taylor GI, Wiesenfeld D. The use of titanium mandibular reconstruction plates in patients with oral cancer. Int J Oral Maxillofac Surg. 1999;28(4):288–90.
4. Wei FC, Celik N, Yang WG, Chen IH, Chang YM, Chen HC. Complications after reconstruction by plate and soft-tissue free flap in composite mandibular defects and secondary salvage reconstruction with osteocutaneous flap. Plast Reconstr Surg. 2003;112(1):37–42.
5. Habijan T, Haberland C, Meier H, Frenzel J, Wittsiepe J, Wuwer C, et al. The biocompatibility of dense and porous nickel–titanium produced by selective laser melting. Mater Sci Eng C. 2013;33(1):419–26.
6. van der Rijt EEM, Noorlag R, Koole R, Abbink JH, Rosenberg AJWP. Predictive factors for premature loss of Martin 2.7 mandibular reconstruction plates. Br J Oral Maxillofac Surg. 2015;53(2):121–5.
7. Lindqvist C, Söderholm AL, Laine P, Paatsama J. Rigid reconstruction plates for immediate reconstruction following mandibular resection for malignant tumors. J Oral Maxillofac Surg. 1992;50(11):1158–63.
8. Maurer P, Eckert AW, Kriwalsky MS, Schubert J. Scope and limitations of methods of mandibular reconstruction: a long-term follow-up. Br J Oral Maxillofac Surg. 2010;48(2):100–4.
9. Paré A, Bossard A, Laure B, Weiss P, Gauthier O, Corre P. Reconstruction of segmental mandibular defects: current procedures and perspectives. Laryngoscope Investig Otolaryngol. 2019;4(6):587–96.
10. Martola M, Lindqvist C, Hänninen H, Al-Sukhun J. Fracture of titanium plates used for mandibular reconstruction following ablative tumor surgery. J Biomed Mater Res B Appl Biomater. 2007;80B(2):345–52.
11. Kimura A, Nagasao T, Kaneko T, Tamaki T, Miyamoto J, Nakajima T. Adequate fixation of plates for stability during mandibular reconstruction. J Cranio-Maxillofac Surg. 2006;34(4):193–200.
12. Farber SJ, Snyder-Warwick AK, Skolnick GB, Woo AS, Patel KB. Maxillomandibular fixation by plastic surgeons. Ann Plast Surg. 2016;77(3):305–7.
13. Liu SP, Cai ZG, Zhang J, Zhang JG, Zhang Y. Stability and complications of miniplates for mandibular reconstruction with a fibular graft: outcomes for 544 patients. Br J Oral Maxillofac Surg. 2016;54(5):496–500.
14. Ahmad M, Nanda R, Bajwa AS, Candal-Couto J, Green S, Hui AC. Biomechanical testing of the locking compression plate: when does the distance between bone and implant significantly reduce construct stability? Injury. 2007;38(3):358–64.
15. Vazquez-Armendariz J, Olivas-Alanis LH, Mahan T, Rodriguez CA, Groeber M, Niezgoda S, et al. Workflow for robotic point-of-care manufacturing of personalized maxillofacial graft fixation hardware. Integr Mater Manuf Innov. 2023;12(2):92–104.
16. ASTM. F382-17 standard specification and test method for metallic bone plates. 2023.

17. Schell H, Duda GN, Peters A, Tsitsilonis S, Johnson KA, Schmidt-Bleek K. The haematoma and its role in bone healing. J Exp Orthop. 2017;4(1):5.
18. Nagasao T, Miyamoto J, Kawana H. Biomechanical evaluation of implant placement in the reconstructed mandible. Int J Oral Maxillofac Implants. 2009;24(6):999–1005.
19. Shayesteh Moghaddam N, Taheri Andani M, Amerinatanzi A, Haberland C, Huff S, Miller M, et al. Metals for bone implants: safety, design, and efficacy. Biomanuf Rev. 2016;1(1):1.
20. Yang C, Abanteriba S, Becker A. A review of shape memory alloy based filtration devices. AIP Adv. 2020;10(6): 060701.
21. Ibrahim H, Jahadakbar A, Dehghan A, Moghaddam N, Amerinatanzi A, Elahinia M. In vitro corrosion assessment of additively manufactured porous NiTi structures for bone fixation applications. Metals. 2018;8(3):164.
22. Farber E, Zhu JN, Popovich A, Popovich V. A review of NiTi shape memory alloy as a smart material produced by additive manufacturing. Mater Today Proc. 2020;30:761–7.
23. Naujokat H, Gökkaya AI, Açil Y, Loger K, Klüter T, Fuchs S, et al. In vivo biocompatibility evaluation of 3D-printed nickel–titanium fabricated by selective laser melting. J Mater Sci Mater Med. 2022;33(2):13.
24. Pilliar RM, Cameron HU, Binnington AG, Szivek J, Macnab I. Bone ingrowth and stress shielding with a porous surface coated fracture fixation plate. J Biomed Mater Res. 1979;13(5):799–810.
25. Chmielewska A, Dean D. The role of stiffness-matching in the design of metallic skeletal reconstruction devices—a review. Bethesda: Acta Materalia, Inc.; 2023.
26. Gallego L, Pérez-Basterrechea M, García-Consuegra L, Álvarez-Viejo M, Megías J, Novoa A, et al. Repair of segmental mandibular bone defects in sheep using bone marrow stromal cells and autologous serum scaffold: a pilot study. J Clin Periodontol. 2015;42(12):1143–51.
27. Watson E, Pearce HA, Hogan KJ, van Dijk NWM, Smoak MM, Barrios S, et al. Repair of complex ovine segmental mandibulectomy utilizing customized tissue engineered bony flaps. PLoS ONE. 2023;18(2): e0280481.
28. Araújo MM, Lauria A, Mendes MBM, Claro APRA, Claro CADA, Moreira RWF. Analysis of residual stress and hardness in regions of pre-manufactured and manual bends in fixation plates for maxillary advancement. Oral Maxillofac Surg. 2015;19(4):369–73.
29. Wan B, Yoda N, Zheng K, Zhang Z, Wu C, Clark JR, et al. On effect of residual stress on fracture behavior of mandibular reconstruction plates. Eng Fract Mech. 2024;305: 110158.
30. Li Y, Li Z, Tian L, Li D, Lu B, Shi C, et al. Clinical application of 3D-printed PEEK implants for repairing mandibular defects. J Cranio-Maxillofac Surg. 2022;50(8):621–6.
31. Suresh V, Anolik R, Powers D. The utility of polyether-ether-ketone implants adjacent to sinus cavities after craniofacial trauma. J Oral Maxillofac Surg. 2018;76(11):2361–9.
32. Moghaddam NS, Skoracki R, Miller M, Elahinia M, Dean D. Three dimensional printing of stiffness-tuned, nitinol skeletal fixation hardware with an example of mandibular segmental defect repair. Procedia CIRP. 2016;49:45–50.
33. Olivas-Alanis LH. Implementation of advanced design and additive manufacturing techniques for the development of medically relevant devices. [Monterrey]: Tecnologico de Monterrey; 2023.
34. Sun Z, Rafferty KL, Egbert MA, Herring SW. Mandibular mechanics after osteotomy and distraction appliance placement I: postoperative mobility of the osteotomy site. J Oral Maxillofac Surg. 2006;64(4):610–9.
35. Wan B, Yoda N, Zheng K, Zhang Z, Wu C, Clark J, et al. On interaction between fatigue of reconstruction plate and time-dependent bone remodeling. J Mech Behav Biomed Mater. 2022;136: 105483.
36. Tadich T, Tarazona AM. Replacement, reduction and refinement: ethical considerations in the current applications of the 3Rs. 2023. p. 667–83.
37. Snihirova D, Höche D, Lamaka S, Mir Z, Hack T, Zheludkevich ML. Galvanic corrosion of Ti6Al4V-AA2024 joints in aircraft environment: modelling and experimental validation. Corros Sci. 2019;157:70–8.
38. Figueira N, Silva TM, Carmezim MJ, Fernandes JCS. Corrosion behaviour of NiTi alloy. Electrochim Acta. 2009;54(3):921–6.
39. Bansiddhi A, Sargeant TD, Stupp SI, Dunand DC. Porous NiTi for bone implants: a review. Acta Biomater. 2008;4(4):773–82.
40. Bocchetta P, Chen LY, Tardelli JDC, dos Reis AC, Almeraya-Calderón F, Leo P. Passive layers and corrosion resistance of biomedical Ti-6Al-4V and β-Ti alloys. Coatings. 2021;11(5):487.
41. Keaveny TM, Clarke BL, Cosman F, Orwoll ES, Siris ES, Khosla S, et al. Biomechanical computed tomography analysis (BCT) for clinical assessment of osteoporosis. Osteoporos Int. 2020;31(6):1025–48.
42. Claes L, Augat P, Suger G, Wilke HJ. Influence of size and stability of the osteotomy gap on the success of fracture healing. J Orthop Res. 1997;15(4):577–84.
43. Korioth TWP, Romilly DP, Hannam AG. Three-dimensional finite element stress analysis of the dentate human mandible. Am J Phys Anthropol. 1992;88(1):69–96.
44. Ma Z, Qiang Z, Zhao H, Piao H, Ren L. Mechanical properties of cortical bones related to temperature and orientation of Haversian canals. Mater Res Express. 2020;7(1): 015408.
45. Mirzaali MJ, Schwiedrzik JJ, Thaiwichai S, Best JP, Michler J, Zysset PK, et al. Mechanical properties of cortical bone and their relationships with age, gender, composition and microindentation properties in the elderly. Bone. 2016;93:196–211.
46. Martini L, Fini M, Giavaresi G, Giardino R. Sheep model in orthopedic research: a literature review. Comp Med. 2001;51(4):292–9.
47. Ravaglioli A, Krajewski A, Celotti GC, Piancastelli A, Bacchini B, Montanari L, et al. Mineral evolution of bone. Biomaterials. 1996;17(6):617–22.
48. den Boer FC, Patka P, Bakker FC, Wippermann BW, van Lingen A, Vink GQM, et al. New segmental long bone defect model in sheep: quantitative analysis of healing with dual energy X-ray absorptiometry. J Orthop Res. 1999;17(5):654–60.
49. Schouman T, Schmitt M, Adam C, Dubois G, Rouch P. Influence of the overall stiffness of a load-bearing porous titanium implant on bone ingrowth in critical-size mandibular bone defects in sheep. J Mech Behav Biomed Mater. 2016;59:484–96.

50. Abu-Serriah M, Kontaxis A, Ayoub A, Harrison J, Odell E, Barbenel J. Mechanical evaluation of mandibular defects reconstructed using osteogenic protein-1 (rhOP-1) in a sheep model: a critical analysis. Int J Oral Maxillofac Surg. 2005;34(3):287–93.
51. Tatara AM, Koons GL, Watson E, Piepergerdes TC, Shah SR, Smith BT, et al. Biomaterials-aided mandibular reconstruction using in vivo bioreactors. Proc Natl Acad Sci. 2019;116(14):6954–63.
52. Jahadakbar A, Shayesteh Moghaddam N, Amerinatanzi A, Dean D, Karaca H, Elahinia M. Finite element simulation and additive manufacturing of stiffness-matched NiTi fixation hardware for mandibular reconstruction surgery. Bioengineering. 2016;3(4):36.
53. Chmielewska A, Jahadakbar A, Wysocki B, Elahinia M, Święszkowski W, Dean D. Chemical polishing of additively manufactured, porous, nickel–titanium skeletal fixation plates. Print Addit Manuf. 2021;9(4):269–77.

Publisher's Note